Spraying Quantum Dot Conjugates in the Colon of Live Animals Enabled Rapid and Multiplex Cancer Diagnosis Using Endoscopy

Youngrong Park,[†,¶] Yeon-Mi Ryu,[‡,¶] Yebin Jung,[†] Taejun Wang,[§] Yeonggyeong Baek,[⊥] Yeoreum Yoon,[∥] Sang Mun Bae,[‡] Joonhyuck Park,[†] Sekyu Hwang,[†] Jaeil Kim,[#] Eun-Ju Do,[‡] Sang-Yeob Kim,[‡,▽] Euiheon Chung,[⊗] Ki Hean Kim,[*,§,∥] Sungjee Kim,[*,†,⊥] and Seung-Jae Myung[*,‡,○]

[†]Department of Chemistry, Pohang University of Science and Technology (POSTECH), San 31, Hyojadong, Nam-gu, Pohang 790-784, South Korea, [‡]Asan Institute for Life Sciences, Asan Medical Center, University of Ulsan College of Medicine, 88 Olympic-ro, 43-gil, Songpa-gu, Seoul 138-736, South Korea, [§]Division of Integrative Biosciences and Biotechnology, Pohang University of Science and Technology (POSTECH), San 31, Hyojadong, Nam-gu, Pohang 790-784, South Korea, [⊥]School of Interdisciplinary Bioscience and Bioengineering, Pohang University of Science and Technology (POSTECH), San 31, Hyojadong, Nam-gu, Pohang 790—784, South Korea, [∥]Department of Mechanical Engineering, Pohang University of Science and Technology (POSTECH), San 31, Hyojadong, Nam-gu, Pohang 790-784, South Korea, [#]Health Screening and Promotion Center, Asan Medical Center, University of Ulsan College of Medicine, 88 Olympic-ro, 43-gil, Songpa-gu, Seoul 138-736, South Korea, [▽]Department of Medicine, University of Ulsan College of Medicine, 88 Olympic-ro, 43-gil, Songpa-gu, Seoul 138-736, South Korea, [⊗]Department of Medical System Engineering and School of Mechatronics, Gwangju Institute of Science and Technology, 123 Cheomdan-gwagiro, Buk-gu, Gwangju 500-712, South Korea, and [○]Department of Gastroenterology, Asan Medical Center, University of Ulsan College of Medicine, 88 Olympic-ro, 43-gil, Songpa-gu, Seoul 138-736, South Korea. [¶]These authors contributed equally.

ABSTRACT The detection of colon cancer using endoscopy is widely used, but the interpretation of the diagnosis is based on the clinician's naked eye. This is subjective and can lead to false detection. Here we developed a rapid and accurate molecular fluorescence imaging technique using antibody-coated quantum dots (Ab—QDs) sprayed and washed simultaneously on colon tumor tissues inside live animals, subsequently excited and imaged by endoscopy. QDs were conjugated to matrix metalloproteinases (MMP) 9, MMP 14, or carcinoembryonic antigen (CEA) Abs with zwitterionic surface coating to reduce nonspecific bindings. The Ab—QD probes can diagnose tumors on sectioned mouse tissues, fresh mouse colons stained *ex vivo* and also *in vivo* as well as fresh human colon adenoma tissues in 30 min and can be imaged with a depth of 100 μm. The probes successfully detected not only cancers that are readily discernible by bare eyes but also hyperplasia and adenoma regions. Sum and cross signal operations provided postprocessed images that can show complementary information or regions of high priority. This multiplexed quantum dot, spray-and-wash, and endoscopy approach provides a significant advantage for detecting small or flat tumors that may be missed by conventional endoscopic examinations and bestows a strategy for the improvement of cancer diagnosis.

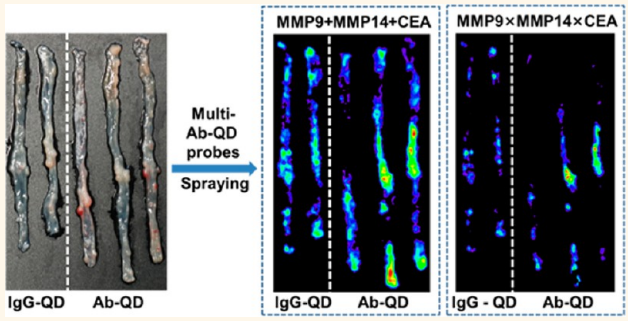

KEYWORDS: quantum dot · imaging probe · nanoparticle · colon cancer · tumor imaging · endoscopy

Colorectal cancer is the second most common cause of cancer-related mortality.[1] Early detection of colorectal cancer with high accuracy is of paramount importance,[2] where colonoscopy is a standard diagnostic tool for colorectal cancer screening and has contributed significantly to reduce mortality.[3] However, colonoscopy sometimes faces difficulties in the rapid and accurate diagnosis, particularly in the cases of chronic inflammation-associated colon tumors. Whereas polypoid lesions are relatively easy to detect by colonoscopy, flat or depressed lesions show higher miss rate. The miss rate for flat adenomas is 42% and over 50% for depressed polyps, while it is 32% for polyps.[4] Colonoscopy is heavily dependent on the observation by naked eyes and the diagnosis is mostly based on the morphology's details such as pit pattern. To better assist the endoscopic diagnosis, many endoscopic techniques have been developed

* Address correspondence to kiheankim@postech.ac.kr, sungjee@postech.ac.kr, sjmyung@amc.seoul.kr.

Received for review February 15, 2014 and accepted September 4, 2014.

Published online September 04, 2014
10.1021/nn5009269

such as chromoendoscopy, narrow-band imaging (NBI) and magnifying endoscopy for precancerous adenomatous lesions.[5−7] Chromoendoscopy is a technique that involves the application of dye molecules to visualize the surface structure of epithelial lesions, and NBI utilizes narrow-band filter to enhance the vasculature visualization within mucosal layer and/or superficial architectures. Magnifying endoscopy is a zoom colonoscopy approach that allows the visualizations of details such as mucosal crypt patterns. Unfortunately, the advances in colonoscopic techniques only show marginal improvement in diagnostic determination of colon polyps, adenomas, or flat adenomas.[8] Histopathologic evaluation of biopsy specimens provides accurate diagnoses; however, it is not compatible with rapid detection such as in operation field and it cannot screen the entire or large portion of colon. To overcome these limitations, there are fierce efforts to develop molecular imaging diagnostic techniques for detecting colon cancer. Gambhir and co-workers have successfully demonstrated the ability to image six surface enhanced Raman spectroscopy (SERS) signals on human colon tissues using gold nanoparticle based SERS probes, which showcased the potential toward a clinically translatable, noncontact Raman endoscope that would be capable of rapidly scanning large and topographically complex tissue surfaces.[9] They have also studied the biodistribution of intrarectally administrated probes in mice by radiolabeling them with ^{64}Cu and imaging them using microPET, which showed localized accumulation in colon followed by the rapid excretion with no appreciable uptake in any other organs.[10] Fluorescence-based molecular imaging is a promising molecular imaging approach because the probes can identify targeted receptors from the emission color, the single can be quantified, and the signal could be enhanced *versus* background signal by selection of probes with appropriate wavelengths. Miller *et al.* reported 5′-fluorescein isothiocyanate (FITC) labeled peptide probe (FITC-QPIHPNNM) for colonic adenoma detection in a mouse model, suggesting the potential for guided detection and resection of cancer.[11]

Quantum dots (QDs) are semiconductor nanoparticles that can be well suited as probes for biomedical imaging because they are bright, photostable, and allow multiplexing by single excitation wavelength.[12−17] QDs have broad absorption profile with large one-photon and two-photon absorption cross sections, narrow and symmetric emission profile, and large effective Stokes shifts. These advantages of QDs in multiplexing can be particularly important in fluorescence molecular imaging of cancer tissues because of the need to image multiple biological targets for improving the accuracy of cancer detection. Single targets may not be useful because of the inherent inhomogeneity of the cancerous tissues. QDs have been exploited for immunohistofluorescence (IHF) detections of multiple cancer markers on formalin-fixed paraffin embedded (FFPE) specimens.[18−24] Li and co-workers used human epidermal growth factor receptor 2 (HER2) antibody (Ab), biotinylated secondary Ab, and QD−avidin conjugate to detect the malignancy of human breast tissues.[18] Liu *et al.* performed double-color imaging using HER2 and type IV collagen in breast cancer tissues.[19] Byers and co-workers showed human ovarian tumor multiplexed detection on FFPE tissues using CD34, Cytokeratin 18, and Caspase 3 sequential staining.[20] Chen and co-workers investigated QD conjugate detection of surgical squamous cell carcinoma in head and neck FFPE specimens using E-cadherin and EGFR sequential staining and reported the sequence dependent signal variance.[21] O'Regan and co-workers reported the multiplexed detection of ER, PR, mTOR, EGFR and HER2 in FFPE human breast cancer specimens with primary Ab−QD conjugates, where the average values of the biomarkers using QD probes were well correlated with immunohistochemistry results.[22] Nie and co-workers reported four-color multiplexed QD conjugates with four protein biomarkers (E-cadherin, high-molecular-weight cytokeratin, p63, and α-methylacyl CoA racemase) mapping on human prostate cancer FFPE sectioned tissue.[23] They performed sequential stainings in which the pretreatment by two primary antibodies from different species was followed by the staining using two secondary Ab−QD conjugates targeting the two primary antibody species. After washing, another two primary antibodies were treated and stained by two secondary Ab−QD conjugates. This sequential staining using different cancer marker primary antibodies from different species reduced the cross-talk, and a single malignant tumor cell could be mapped and identified from the complex tissue microenvironment.

Herein, we report the use of Ab−QD conjugates for multiplexed colonoscopic cancer detection. Primary Ab−QD conjugates were chosen for "spray and wash" type applications which eliminate lengthy procedures. The spray and wash procedure adopts topical introduction of primary Ab−QD conjugates by a spraying catheter which is followed by a vigorous washing step and the remaining targeted Ab−QD probes were directly monitored. Sequential secondary Ab−QD conjugate staining by different species origin may provide ample cellular level information but with the time cost over hours. Typically, primary Ab−QD conjugates are known to be less specific than the staining using the secondary Ab−QD conjugates on tissues pretreated with primary Ab. Wang and co-workers have also observed this as they image oropharyngeal squamous cell carcinomas with FFPE tissues.[24] Zwitterionic QD surface coating has been exploited to overcome the specificity issue of primary Ab staining, which provides minimal nonspecific bindings.[25,26] Fresh intact tissues have been tested as well as FFPE sectioned

tissues to confirm the applicability to colonoscopy. Another advantage of using a spray and wash procedure is that this reduces the potential toxicity of QDs. Cd-containing QDs were used for this study as a proof-of-concept experiment; however, less toxic QDs such as InP/ZnS (Core/Shell), ZnTe/ZnSe (Core/Shell), $CuInS_2$/ZnS (Core/Shell), and Ag_2S QD would be desirable for future clinical translation.[27−29] Multicolor Ab−QD probes were prepared using colon cancer markers of carcinoembryonic antigen (CEA), matrix metalloproteinase (MMP) 9 and MMP 14, which are markers for cancer progression and metastasis.[30−35] CEA is a cell membrane glycoproteins for cell adhesion. CEA is one of most commonly used biomarkers in colon cancer and the serum CEA level has been accepted as a prognostic indicator in colorectal cancer patients.[36] MMPs are membrane-associated or excreted and are involved in tumor invasion and metastasis. The expression of MMPs on the tumor cells and the microenvironment of the host stroma contributes to tumor growth at advancing stages in colon carcinoma.[37] Expression levels of MMP9 in malignant colorectal tumors have been reported to increase significantly when compared with normal tissues, however the overexpression level was reported to not directly correlate with tumor stage.[38] On the other hand, MMP14 expression level was reported to show correlated increase from normal to adenoma, and carcinoma.[39] In addition, these biomarkers are suitable for our spray and wash application because they are mostly located on the external surfaces of cells and are accessible by target biomarkers. CEA is known to heavily populate along the luminal surfaces of malignant colon cells.[40,41] Overexpressions of MMPs are expected at the peripherals of tumors, which may well reach the luminal surfaces. We have evaluated the cancer detection capability by our multicolor QD−Ab conjugate probes in sectioned mouse colon tissues and also in *ex vivo* and *in vivo* stained fresh mouse colon tissues treated by spraying staining method. Postimage processes such as sum or cross operation of different probes have been demonstrated to maximize the utility of multiplexing and reduce false negative or false positive errors. To investigate the spatial distribution of the probes in colon tissue, two-photon microscopic imaging was performed for the *ex vivo* and *in vivo* Ab−QD probe stained tissues. The simultaneous multicolor detection has been further extended to human colon adenoma species, showcasing the possibility of rapid and accurate colonoscopic diagnosis using our QD−Ab conjugate probes.

RESULTS AND DISCUSSION

Preparation of Ab−QD Probes and the Control with Normal IgG. Three different color emitting CdSe/CdS/ZnS (Core/Shell/Shell) QDs were synthesized using procedures previously published (see Experimental Section for details).[25] The absorption and fluorescence profiles are shown in Figure 1, where the emission peaks can be found at 560, 585, and 630 nm (noted as 560QD, 585QD, and 630QD, respectively). The QD surface was co-decorated with a zwitterionic ligand and a ligand bearing carboxylic acid as described in our previous publication.[25] The carboxylic acids were used for conjugation with MMP9, MMP14, or CEA antibody using the conjugation protocol described in our previous publication.[25] The isotype normal immunoglobulin G (IgG) antibody was used for the control (See Experimental Section for details). After the antibody conjugation, ~7 nm increase in the hydrodynamic size was measured by dynamic light scattering (Figure S1). We have also performed gel-electrophoresis for unconjugated 630QD and MMP9−630QD conjugate samples to confirm the absence of unconjugated QD probes after the conjugation reaction (Supporting Information Figure S2). Cytotoxicity assays were performed by measuring the mitochondrial activity, and no noticeable cytotoxicity was observed for up to 600 nM probe for 24 h (Supporting Information Figure S3). We have confirmed the affinities of our MMP9−630QD, MMP14−630QD, CEA−630QD conjugate probes against normal IgG−630QD conjugates using known positive and negative cell lines of MMP9, MMP14, and CEA (Supporting Information Figure S4). The cell-specificity experiments confirmed the specificity of our MMP9, MMP14, and CEA QD probes.

Ab−QD Probe Staining for Sectioned AOM/DSS Mouse Colon Tissues. Azoxymethane/dextran sodium sulfate (AOM/DSS) mouse model was prepared using BALB/c mice (see the Experimental Section for details). The colons of AOM/DSS treated mice were removed, dissected longitudinally, fixed with 10% formalin and then embedded in paraffin. Tissues were sectioned into 4 μm slices. For the staining with Ab−QD probe, deparaffinization, rehydration and antigen retrieval of tissue were followed (see Experimental Section for details). Four Ab−QDs were prepared using 630 nm emitting QDs conjugating to CEA, MMP9, MMP14, or normal IgG control. Normal IgG antibodies are typical negative control for immunohistochemistry because they have corresponding control isotype and thus can evaluate the nonspecific bindings of Ab−QD probes. Different Ab conjugates with 630QD were used for the FFPE tissue staining to measure the specific binding level of each Ab−QD probe. Single color monochannel-(targeting one marker) staining was performed to validate the antibody targeting as being independent from the QD probe color dependence. Each Ab−QD conjugate PBS solution (1 μM) was sprayed onto the pretreated tissues and incubated for 1 h. Figure 2 shows the overall schematic of our experiments which can be categorized into (i) *ex vivo* staining of sectioned colon tissues using single Ab−QD probe, (ii) *ex vivo* staining of fresh colon tissues using single Ab−QD

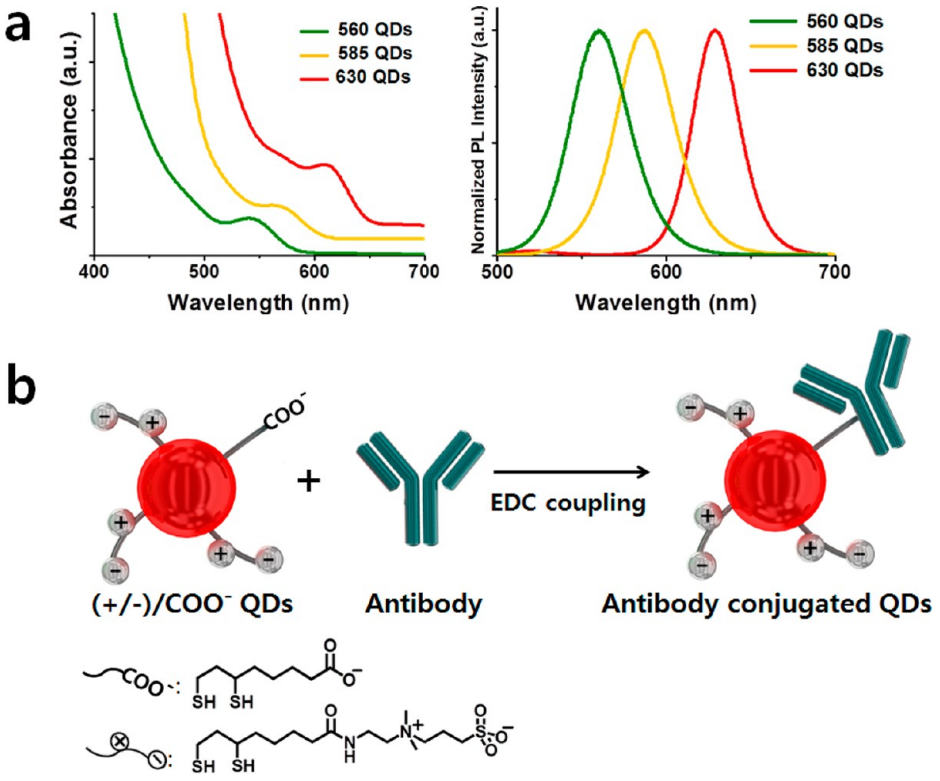

Figure 1. (a) Absorption and fluorescence profiles of the quantum dots 560QD, 585QD, and 630QD. (b) Scheme for antibody−QD conjugation. The QD surface was co-decorated with a zwitterionic ligand (+/−) and a ligand bearing carboxylic acid (COO^-). The carboxylic acid was used for conjugation with antibody using carbodiimide couping.

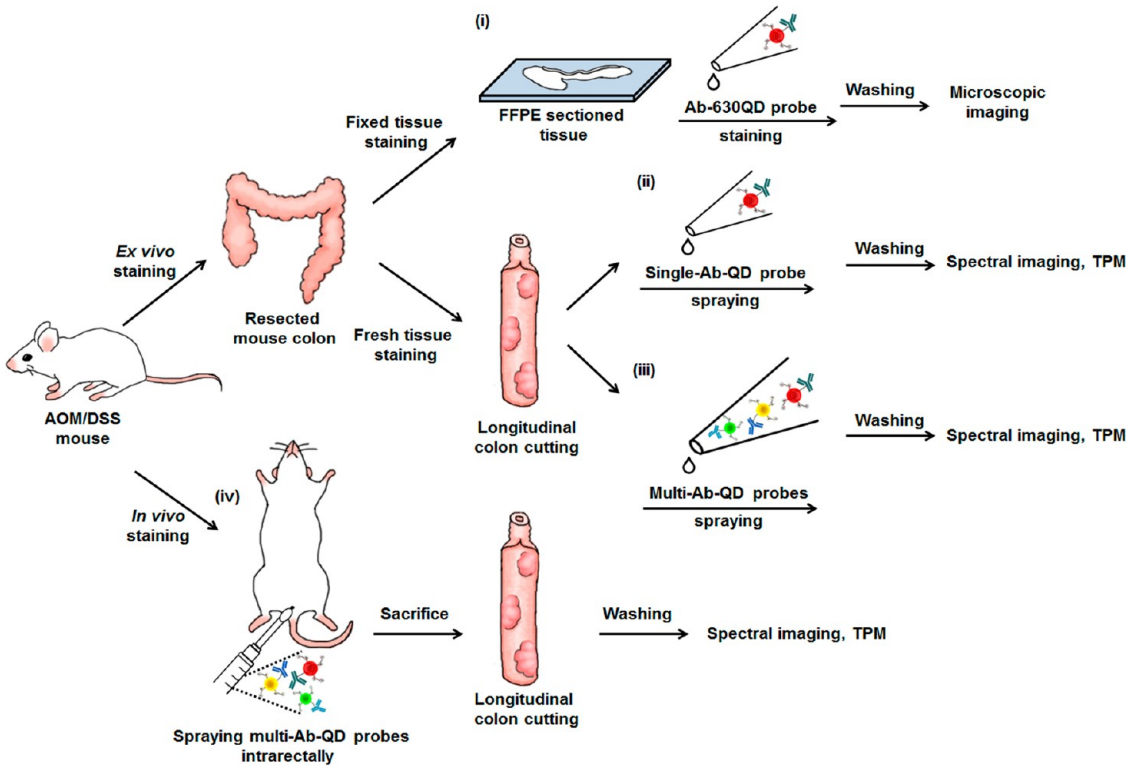

Figure 2. An illustrated schematic showing four categories of the performed experiments using AOM/DSS colon cancer mouse model: (i) *ex vivo* staining of sectioned colon tissues using single Ab−QD probe, (ii) *ex vivo* staining of fresh colon tissues using single Ab−QD probes, (iii) *ex vivo* staining of fresh colon tissues using multi Ab−QD probes, and (iv) *in vivo* staining by intrarectal spraying using multi Ab−QD probes. TPM = Two-Photon Microscopy.

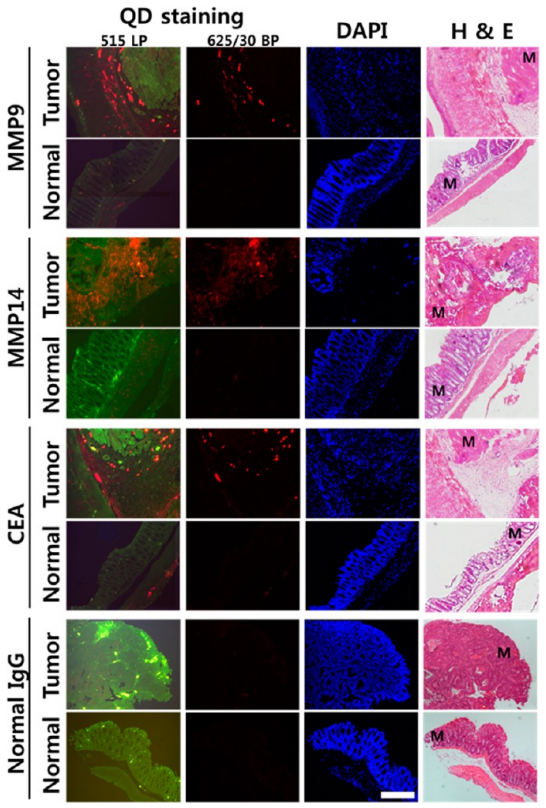

Figure 3. Representative fluorescence microscope images of sectioned AOM/DSS mouse colon tissues that have been stained by MMP9−630QD, MMP14−630QD, and CEA−630QD probes. Tumor tissues (top row of each panel) and normal tissues (bottom row of each panel) were stained by the MMP9−630QD, MMP14−630QD, CEA−630QD, or by the control IgG QD probe (panels from top to bottom). Fluorescence images were taken using 515 nm long pass emission filter (first column) or using 625/30 nm band-pass filter (second column). DAPI (third column) and H&E (last column) staining were also obtained. M: mucosa. Scale bar = 200 μm.

probes, (iii) *ex vivo* staining of fresh colon tissues using multi Ab−QD probes, and (iv) *in vivo* staining by intrarectal spraying using multi Ab−QD probes. Figure 3 shows the representative fluorescence microscope images of sectioned mouse colon tissues that have been stained by each Ab−QD probe. The tissues were also nuclear stained by 4,6-diamidino-2-phenylindole (DAPI). Traditional hematoxylin and eosin (H&E) staining was also performed for adjacent sectioned tissues for the classification of tumor and normal regions. As shown by the H&E stain in Figure 3, mucosa and adjacent muscles could be distinguished by their morphology. At the first column in Figure 3, fluorescence images were taken with 515 nm long pass filter to simultaneously show the green autofluorescence and red QD signal, where the autofluorescence helped visualize the tissue structures. For all the MMP9, MMP14 or CEA Ab−QD stained tissues, red QD signals can be found with higher intensities at tumor tissues over the normal controls. The QD signals in tumor tissues could be mostly found at mucosa layers. On the contrary, IgG control QD stained tissues did not show

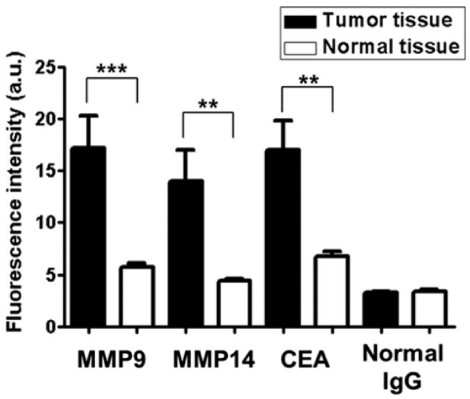

Figure 4. Fluorescence signal mean intensities from the mouse tumor colon tissues (filled bars) and from the normal tissues (empty bars) when stained with MMP9, MMP14, CEA, or normal IgG QD probes (from left to right). Error bars represent the standard error of the mean (*$P < 0.001$, **$P < 0.01$).**

noticeable QD signals irrespective of either the normal or tumor tissues. For accurate QD signal quantifications, the emission filter was switched to 625/30 nm band-pass that selectively collects signals from the 630QD. In the second column of Figure 3, only tumor tissues that have been stained by Ab−QD probes glow brightly with emission from the QDs, whereas normal tissues stained by Ab−QD probes and tumor/control tissues stained by control IgG−QD probes did not. Figure 4 shows the quantitative mean fluorescence intensities between tumor and normal tissue at each biomarker probe and the control probe staining. The QD signal ratios over the normal tissues were 3.0 for MMP9, 3.2 for MMP14, and 2.5 for CEA. The control IgG QD signals showed similar levels for the tumor and normal, which was also similar to the signal levels of normal tissues stained by Ab−QD probes. Our Ab−QD and IgG−QD probes share zwitterionic surface coating, which may have provided the similar and low nonspecific binding level. The results in Figures 3 and 4 validate the selection of our biomarkers. Various biomarkers have been studied in murine model such as AOM/DSS induced inflammation-related mouse model. Shang *et al.* reported that AOM/DSS treated mice showed enhanced production of MMP9 mRNA and the expression level was 4-fold higher than the normal animal.[42] Suzuki *et al.* investigated that MMP14 genes are markedly up-regulated over 3.2 times in AOM/DSS mouse model.[43] Our three Ab−QD probes showed around 3-fold higher signals over the nonspecifically bound controls or over the IgG−QD control staining, which is surprisingly promising considering the relatively short incubation time of 1 h and the direct one-time staining with primary Abs. Mucosa layers, which are accessible from endoscope, showed a high tumor to normal contrasts with Ab−QD staining, which suggests the potential of our Ab−QD probes for a colonoscopic diagnostic agent by "spray and wash" method.

Spray and Wash Single-Ab–QD Probes *ex Vivo* Staining. To investigate the applicability of our Ab–QD probes for "spray and wash" colon staining, fresh intact colon tissues were obtained from AOM/DSS mouse model by surgically excising and longitudinally cutting to expose the mucosa layer of colon immediately after the sacrifice. The colon tissues were typically ~9 cm long. Three different color emitting QDs were used for the Ab conjugation: MMP9 Ab conjugated to 630QD, MMP14 Ab conjugated to 585QD, and CEA Ab conjugated to 560QD. Normal IgG QD conjugates were also prepared as a control probe with each three QDs. The fresh colon tissues were sprayed by 500 nM Ab–QD conjugate probe PBS solution, incubated for 30 min, and washed with PBS buffer for 15 min (see Experimental Section for details). Five mice were sacrificed for each biomarker experimental set to display two whole colons stained by the control IgG–QD conjugate and three colons stained by the Ab–QD probe. The five colons were imaged simultaneously by IVIS imaging system and spectral unmixing was used to select the QD signal and minimize the effect from autofluorescence (see Experimental Section for details). White light images were taken to visualize the colons, and the black and white colon images were overlaid with IVIS images of each probe (Figure 5). MMP9 and MMP14 QD probes showed 1.40 and 1.77 times higher signal levels than the cases of IgG–QD control (The average fluorescence intensities and standard deviations can be found in a table at Supporting Information Figure S5). However, CEA QD probe did not show meaningful signal difference over the control. The staining was also inhomogeneous among different tumor sites. In the case of MMP9 probe, tumors discernible at the white light image were mostly stained by the QD probe. However, the largest tumor polyp (indicated by arrow 1 in Figure 5a) was missed. Presumably, the outer layers of large tumors are less available for the QD probes to infiltrate and/or due to the heterogeneity in biomarker expression level of the tumor. The MMP9 probe may be somewhat specific, however the targeting was not statistically meaningful considering the p value (Supporting Information Figure S5). MMP14 probe showed better results clearly displaying most of the tumor sites with the contrast of very little background signals for the case of the IgG control. The CEA probe showed only marginal tumor targeting capability; the tumors at the rightmost colon were spotted but many tumors at other colons were missed (arrows 2 and 3 in Figure 5c). Some regions showed high probe signals, yet were not easily discernible as cancer or adenoma. Four such representative regions were selected and H&E histological analysis was performed (see Supporting Information Figure S6 for the H&E images). Three regions stained by the MMP14 probe were revealed as hyperplasia (two arrows with the letter "h′" and "h″" in Figure 5b) or

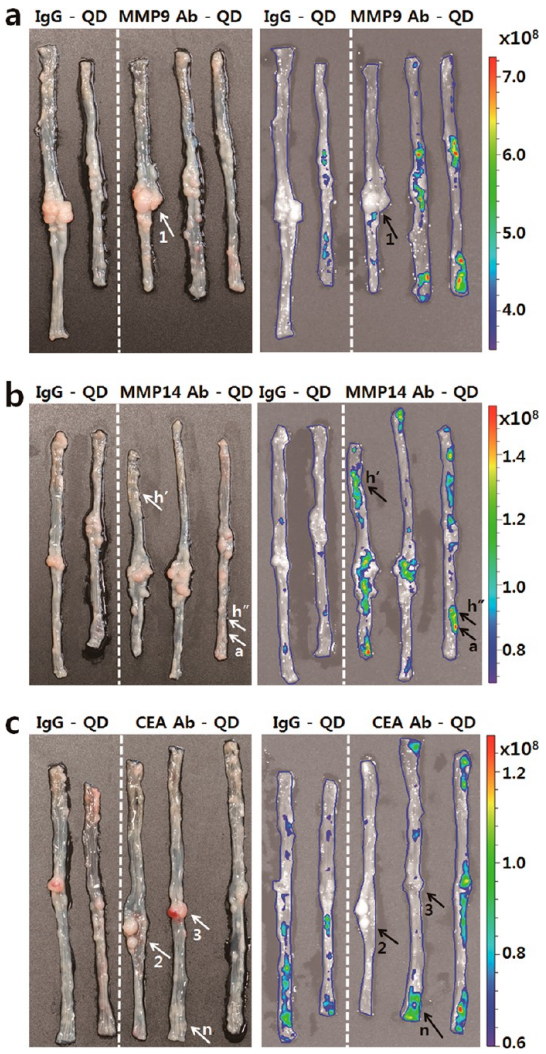

Figure 5. White light images (left panels) and merged pseudocolor IVIS images (right panels) of five juxtaposed colons with the left two stained by IgG–QD control probes and the right three stained by MMP9–630QD (a), MMP14–585QD (b), or CEA–560QD probe (c). The IgG–QD treated colons were separated from the Ab–QD treated colons by the white dotted lines. The areas of region-of-interest (ROI) were indicated by blue lines. Three representative large tumor polyps missed by the probe are indicated by the numbered arrows. Four representative signal regions have been histopathologically analyzed and indicated by arrows with the letters 'h', 'a', and 'n' corresponding to the regions of hyperplasia, high grade adenoma, and normal, respectively.

as high grade adenoma (an arrow with the letter 'a'). This demonstrates the capability of our probe to detect early cancers that can be otherwise only diagnosable by time-consuming histopathological methods. One region stained by the CEA probe was identified as normal (an arrow with the letter 'n'). Considering the high rate of false negative by the CEA probe, the false positive was confirmed using histopathology and the signals can be attributed to nonspecific adsorption of the QD probes. The overall CEA probe signal level was low and had become similar to that of the control IgG–QD. The discrepancy between the FFPE tissues

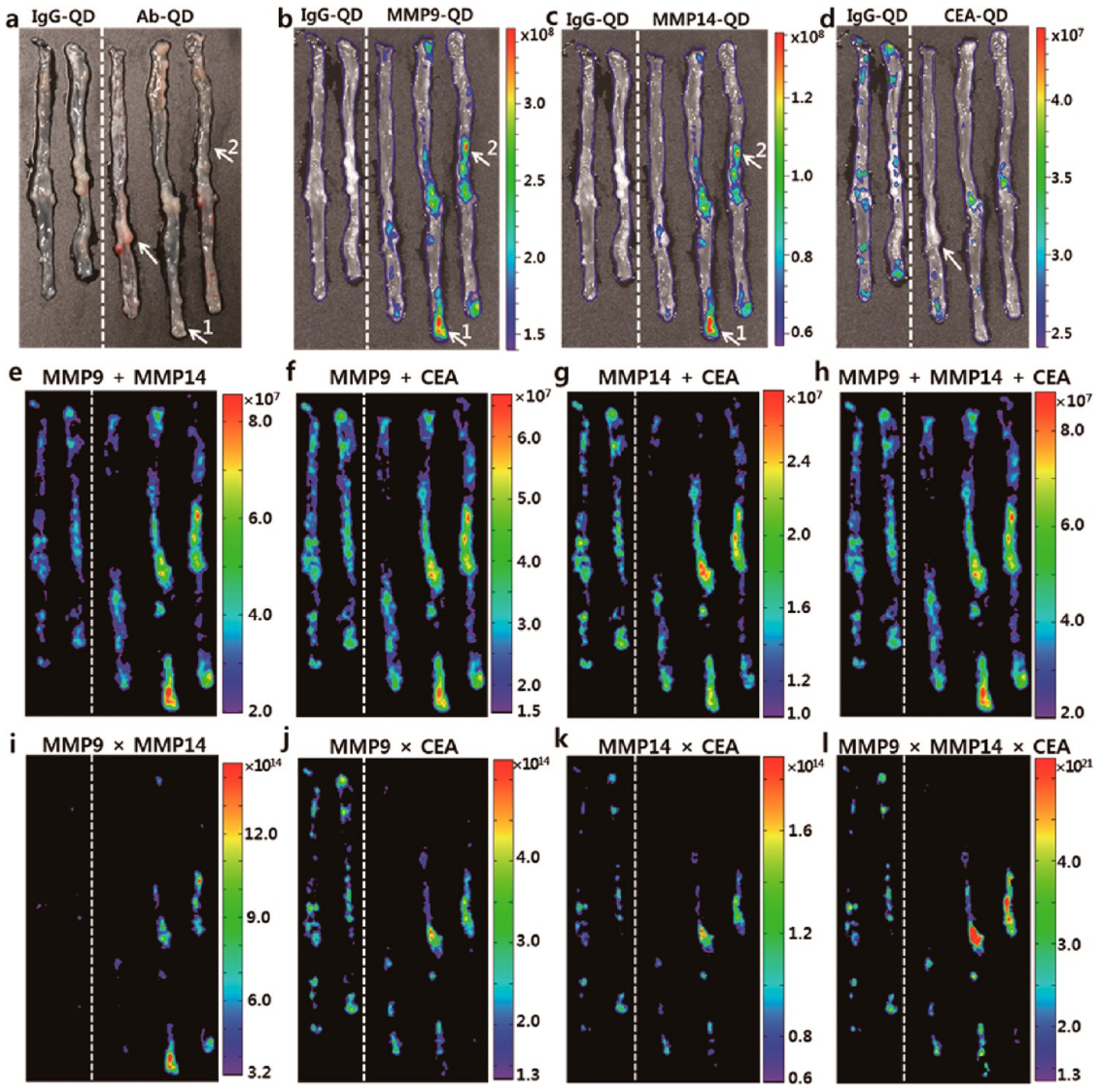

Figure 6. White light images (a) and merged pseudocolor IVIS images (b–d) of five juxtaposed colons with the left two simultaneously stained by IgG–QD control probe of the mixture of IgG–630QD, IgG–585QD, and IgG–560QD and the right three simultaneously stained by multi-Ab–QD probes of the mixture of MMP9–630QD, MMP14–585QD, and CEA–560QD. Signals from 630QD (b), 585QD (c), and 560QD probe (d) were unmixed by the IVIS system for the merged pseudocolor images. The IgG–QD treated colons were separated from the Ab–QD treated colons by the white dotted lines. The areas of region-of-interest (ROI) were indicated by blue lines. QD signal pseudocolor images after the postimage processes by sum operations using the channels of MMP9 + MMP14 (e), MMP9 + CEA (f), MMP14 + CEA (g), and MMP9 + MMP14 + CEA (h) and by cross operations using the channels of MMP9 × MMP14 (i), MMP9 × CEA (j), MMP14 × CEA (k), and MMP9 × MMP14 × CEA (l). The numbered arrows represent regions identified as low grade adenoma by histopathological analysis. The black lines in the rainbow scale represent the signal threshold.

and fresh tissues by identical Ab–QD probes may attribute to the accessibility of the probe. The sectioned FFPE tissues should be equally accessible for the probe from the luminal surface down to the submucosa, however for the fresh tissue staining, the Ab–QD probes need to permeate from the mucosal surface. For rapid and accurate colonoscopic diagnosis, multiplexed probe imaging should be essential because any single probe may fail to diagnose the disease.

Spray and Wash Multi-Ab–QD Probes *ex Vivo* Staining. Since sequential staining does not allow rapid detection, we have further extended our experiments for multiplexed simultaneous staining using the mixture of the three Ab–QD probes (Figure 6). The 500 nM MMP9–630QD, MMP14–585QD, and CEA–560QD solutions were mixed in equal volumes. The final concentration of each probe was 167 nM. Using the mixture probe solution, the fresh colon staining experiment was repeated. As a control to the multi-Ab–QD probe mixture, multi-IgG–QD control probe was prepared by mixing the IgG conjugates of 560QD, 585QD, and 630QD. IVIS spectral imaging was used to measure each probe signal (see Experimental Section for details). The multiplexed staining showed similar results as the single probe staining. MMP9 and MMP14 Ab–QD probes showed distinctive signals at tumor sites that

contrasted well with the small nonspecific bindings by the IgG−QD control. The MMP9 and MMP14 QD probes showed 1.87 times higher signal than the IgG−QD control (The average fluorescence intensities and standard deviations can be found in a table at Supporting Information Figure S7). Two representative regions were selected where the MMP9 and MMP14 probes showed high signal levels, yet they were not easily discernible as adenoma or cancer under white light image. Histopathological analysis identified the regions as low grade adenoma (numbered arrows in Figure 6; see Supporting Information Figure S8 for the H&E images). CEA probe was not properly functioning, where the nonspecific IgG control case showed slightly higher signals at the tumor sites than the probe (Supporting Information Figure S7).

Postimage Processes Using Sum Operation and Cross Operation. The inherent heterogeneity of tumors cells and microenvironment at various cancer stages necessitates doctors to cross-check the results from a single probe label with other probes. This can lead to false or misdiagnosis. Here we show we can overcome this problem by using QD multiplex labeling and analysis. As a proof-of-concept, we have performed the simultaneous multiplexed three Ab−QD probes staining. Information by the three channels was postimage processed using combinations of sum operation and cross operation. Probe signal intensity was normalized for each color probe characteristics such as QD absorbance, photoluminescence quantum efficiency, and detector sensitivity. Each color signal intensity was normalized to be only proportional to the number of the bound Ab−QD probe (see Supporting Information Figure S9 for the experiments performed to obtain the normalization factors). For the sum operation (+), each normalized probe signals at each image pixel were added (see Experimental Section for details). For the cross operation (×), the signals were multiplied to each other instead of the addition. Four combinations were made for each operation: MMP9 + MMP14, MMP9 + CEA, MMP14 + CEA, and MMP9 + MMP14+CEA for the sum operations and MMP9 × MMP14, MMP9 × CEA, MMP14 × CEA, and MMP9 × MMP14 × CEA for the cross operations (Figure 6). These sum operated images complemented missing tumors by each probe, potentially reducing false negative errors. For an example, a tumor site missed by the CEA probe (arrow in Figure 6d) has been complemented after the sum operations. Cross operated images showed more focused spots where different probes colocalize, providing the higher priority regions for attention. These operations are simple and can be easily combined with an endoscopy providing real-time guidance images on the monitor during surgical resection.

Two-Photon Microscopic Imaging of the *ex Vivo* Stained Colon Tissues. As we topically administer the probes onto the fresh colon tissues by the "spray and wash" method, the staining should be critically limited by the depth-dependent distribution of the probes that may be dependent on the tissue-specific permeation and diffusion. To investigate the probe distribution of our Ab−QD probes, two-photon microscope imaging was performed for the *ex vivo* multi-Ab−QD probe stained tissue. A representative tumor tissue was two-photon imaged by 780 nm excitation. The 780 nm excitation was used to visualize the tissue architectures by the autofluorescence. Disordered morphologies were identified for the tumor tissue, whereas the control normal tissue exhibited neat colonic crypts. Considering the crypt of normal tissue, our depth profile is thought limited to the mucosa layer and not reaching the submucosa. For each Ab−QD probe depth-profiling, excitation wavelength was switched to 980 nm to reduce the autofluorescence background and band-pass filter was inserted according to each probe signal detection. Two-photon microscope images were recorded moving down to the *z*-direction from the colonic tissue surface reaching over 100 μm in depth (Figure 7; more photos can be found in Supporting Information Figure S10, and movie clips can be found in Supporting Information). QD signals showed stark contrast between the tumor tissue and the control normal. This contrast is thought to originate from the difference in permeability across the colon epithelial barriers between tumor and normal. Inflammations and tumorigenesis are known to compromise the colon top layers as the tight junctions in the epithelial barriers dysfunction. Colon cancers are reported to suppress protein expression levels essential for the tight junctions.[44,45] The increase in permeability across colon epithelium barriers are also typically found in villus adenoma and adenomatous polyps with increased numbers of aberrant colonic crypts.[46] In tumor, three different Ab−QD probes were well colocalized each other, which indicates three biomarker expressions share the distribution pattern. All the probes showed strong signals at the depth of over 20 μm from surface. Presumably, the epidermal surface does not express as many biomarkers as for the tissues in deeper mucosa. The QD signal continued to 100 μm and began to dim for further depth, which was mostly limited by the two photon microscope instrumental imaging depth. Similar imaging depth can be found for the 780 nm excitation autofluorescence images. Smaller number of probes may have reached to deeper tissues and may have contributed to the signal attenuation in depth-profile. As the control, the two-photon microscopic imaging experiment was repeated using multi-IgG−QD probes (Supporting Information Figure S11, movie clips can be found in Supporting Information). No noticeable signals were found regardless of the detection channel and the tissue depth. Considering our one-time incubation of multi-Ab−QD probe for only 30 min, the staining depth over 100 μm from surface is promising for its future endoscopic applications.

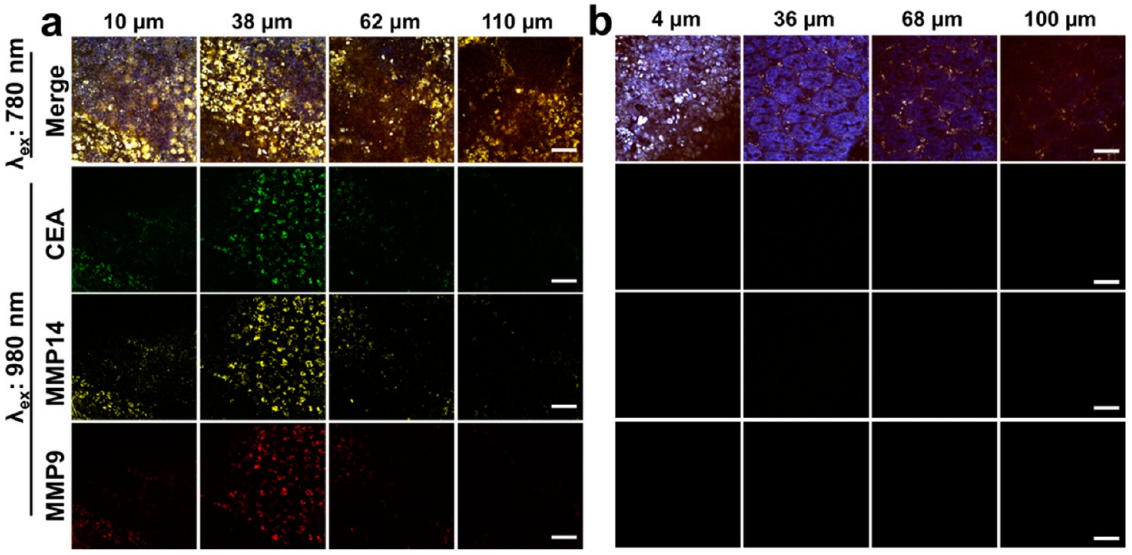

Figure 7. Two-photon microscopic fluorescence images of mouse tumor (a) and normal (b) tissues *ex vivo* stained by spraying multi-Ab−QD probes. Two-photon microscope images were recorded moving down to the *z*-direction. First row shows the autofluorescence imaging by 780 nm excitation. Second to fourth rows represent images by 980 nm excitation, and the emission range was set for 544−560 nm for CEA−560QD probe (second row), 576−596 nm for MMP14−585QD probe (third row), and 620−644 nm for the MMP9−630QD probe (fourth row). Objective = 20×. Scale bar = 50 μm.

Comparison Studies between QD and Rhodamine B Probes. 'Spray and wash' staining by the Ab−QD probes has successfully visualized tumors at fresh colons from AOM/DSS mouse model. Since Ab−organic dye probes are a conventional golden standard for fluorescence-based targeted imaging, we performed a head-to-head comparison between MMP14−585QD probe with MMP14−Rhodamine B conjugate probe (MMP14−Rh). MMP14 Ab was chosen because it performed best among the three Abs for *ex vivo* staining. Rhodamine B dye was selected because it has a relatively high quantum yield and its emission profile (peak at 575 nm) overlaps well with the 585QD (see Experimental Section for the preparation protocol of MMP14-Rh. Absorption and emission spectra of MMP14-Rh can be found at Supporting Information Figure S12). We have repeated the fresh mouse colon staining with Ab−Rh and Ab−585QD probes. Each probe was sprayed onto the fresh mouse colon tissues and incubated for 30 min, which was followed by washing. Under the IVIS imaging, both QD and Rh probes can visualize the tumors that were discernible with white light imaging (Supporting Information Figure S13). Two-photon microscopic imaging experiments were also performed for each probe staining against the tumor and normal tissues to investigate the probe distributions (Supporting Information Figure S14, movie clips can be found in Supporting Information). A 780 nm excitation was used for "merged" images, showing the tissue architectures by the autofluorescence and probe signals from QDs or from Rh dyes. Tumor tissues showed disordered morphologies, whereas the control normal tissue exhibited neat colonic crypts. For QD or Rh probe depth-profiling, excitation wavelength was switched to 980 nm and band-pass filter was inserted. Two-photon microscope images were recorded moving down to the *z*-direction from the colonic tissue surface. In tumor, Ab−QD and Ab−Rh probes shared similar distribution patterns. Both probes showed signals up the depth approaching 100 μm from surface. The depth-dependent signal levels for both probes showed similar fluorescence profiles with the peaks at around 50 um (see Supporting Information Figure S15 for the depth-profiling graphs). Under the identical staining condition, the QD probe may have been slower in diffusing to the targets from the surfaces than the dye probe. However, this seems to have been overcome by the brightness of the QD probe and have resulted in the similar depth-profiles. This demonstrates the potential advantages of rapid and multiplexed QD probe imaging over conventional dye probes. In the case of normal tissues, the 780 nm excitations produced a blue signal visualizing the morphologies from the tissue autofluorescence, but the 980 nm excitation probe channel showed negligible signal levels regardless of the depths.

Mouse Colon Tissue Imaging by "Spray and Wash" Ab−QD Probe *in Vivo* Staining and Two-Photon Microscopic Imaging. The Ab−QD probe "spray and wash" staining has been demonstrated using fresh colons from AOM/DSS mouse model. However, the colons have been stained *ex vivo* and the probe distribution may vary when applied to live animals. For example, the native absorbing function of colon and its movement may increase the background signals at normal tissues by nonspecific binding or uptake. We have repeated the multi-Ab−QD probe AOM/DSS mouse model colon staining experiment as replacing the *ex vivo* staining protocol with that of *in vivo*. The mice were intrarectally

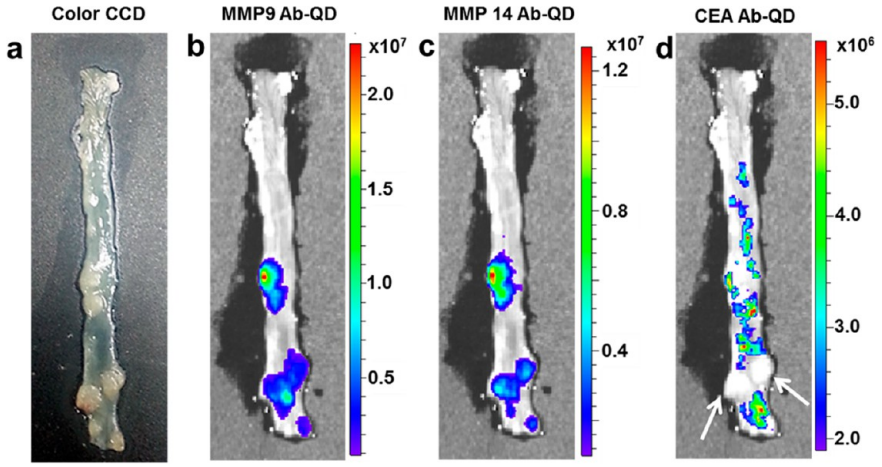

Figure 8. White light images (a) and merged pseudocolor IVIS images (b–d) of a colon *in vivo* stained by multi-Ab–QD probe of the mixture of MMP9–630QD, MMP14–585QD, and CEA–560QD. Signals from 630QD (a), 585QD (b), and 560QD probe (c) were unmixed by the IVIS system for the merged pseudocolor images.

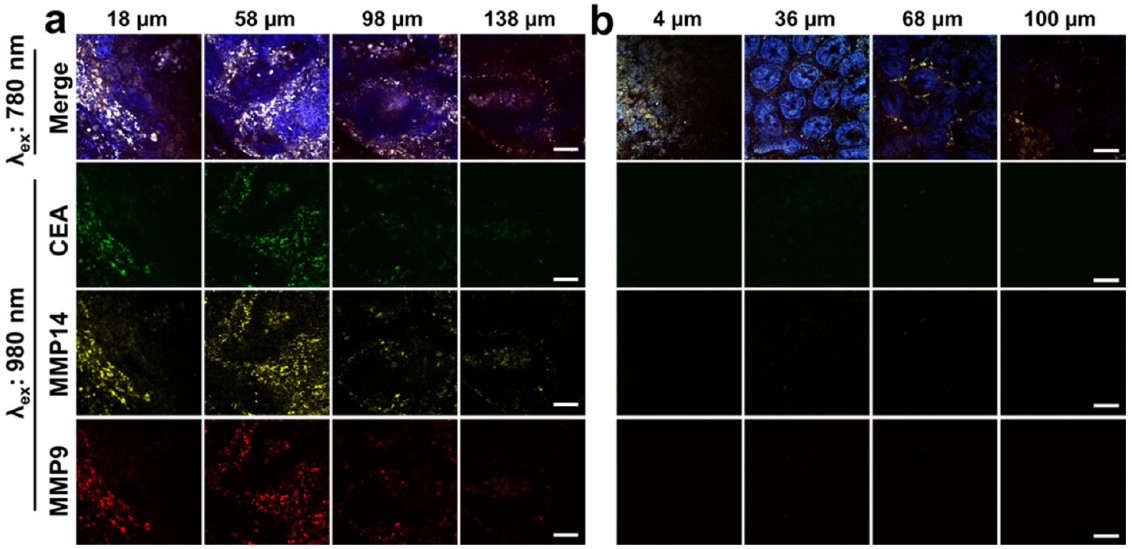

Figure 9. Two-photon microscopic fluorescence images of mouse tumor (a) and normal (b) tissues *in vivo* stained by spraying multi-Ab–QD probes. Two-photon microscope images were recorded moving down to the *z*-direction. First row shows the autofluorescence imaging by 780 nm excitation. Second to fourth rows represent images by 980 nm excitation, and the emission range was set for 544–560 nm for CEA-560QD probe (second row), 576–596 nm for MMP14–585QD probe (third row), and 620–644 nm for the MMP9–630QD probe (fourth row). Objective = 20×. Scale bar = 50 μm.

sprayed with the multi-Ab–QD mixture probes using a syringe with a pliable plastic gavage needle, incubated for 30 min, and then sacrificed to excise the colon for imaging (see Experimental Section for details). For the *in vivo* stained colon, white light image and overlaid IVIS images were shown in Figure 8. The MMP9– and MMP14–QD probes clearly indicated tumor sites while other normal regions were very low in the signal. The CEA–QD probe showed unrelated signal pattern and no signal in the two large tumors (arrows in Figure 8d). These results reflect those of *ex vivo* staining experiments, where the CEA probe failed for our "spray and wash" application in AOM/DSS mouse model. Two-photon microscopic imaging experiment was also repeated for the *in vivo* stained tissues. The 780 nm autofluorescence imaging differentiated the disordered tumor tissue and normal tissue, and each Ab–QD probe distribution was investigated using 980 nm excitation (Figure 9; more photos can be found in Supporting Information Figure S16, and movie clips can be found in Supporting Information). The colocalization of three probes, signal intensities, and depth profiles were almost identical to those of *ex vivo* tumor tissue, showing the signal depth up to 120 μm. Background signal level at the normal tissue was also similar to those of *ex vivo* tissues. The experiment was repeated using the control multi-IgG–QD probes, where no noticeable signals were found regardless of the detection channel and the tissue depth (Supporting Information Figure S17, movie clips can be found in Supporting Information). Apparently, live staining condition did not alter the probe distribution or the nonspecific uptake when the

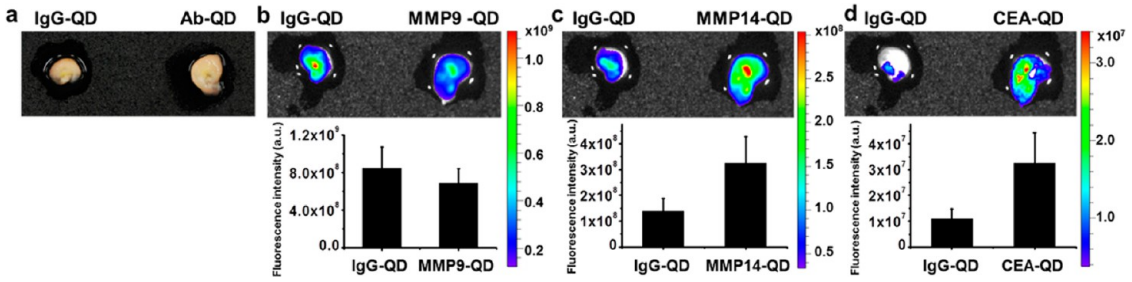

Figure 10. (Top) White light images (a) and merged pseudocolor IVIS images (b–d) of a human colon adenoma specimen stained with multi-Ab–QD probe of the mixture of MMP9–630QD, MMP14–585QD, and CEA–560QD (left) or control IgG–QD probe of the mixture of IgG–630QD, IgG–585QD, and IgG–560QD (right). (Bottom) Average fluorescence signal intensities from the human colon adenoma specimen. Signals from 630QD (b), 585QD (c), and 560QD probe (d) were unmixed by the IVIS system for the merged pseudocolor images.

colon is active and functioning such as water absorption process of the large intestines. This may attribute to the short staining time of 30 min and slowed colon functions when the animal is under anesthesia. Conventional human colonoscopy is also frequently accompanied by drugs inhibiting gastrointestinal movements, which can potentially minimize nonspecific uptakes.

Human Colon Tissue Imaging by "Spray and Wash" Ab–QD Probes. We have further applied our multi-Ab–QD mixture probe to human colon adenoma specimen from the clinic. A colon adenoma excised from patients was cut in half to compare the multi-Ab–QD probe staining with the multi-IgG–QD control probe. A 330 nM multi-Ab–QD mixture probe solution was sprayed onto the tissues, and the samples were incubated for 60 min, followed by washing for 3 min. Figure 10 shows the white light image and overlaid IVIS images showing each probe and control probe signals. MMP14 and CEA probes showed meaningfully high signals when compared to normal IgG control probe, whereas the MMP9 probe did not significantly differ in the signal intensity from the IgG control. The experiment was repeated with three different polyps from patients, and each probe intensity over the same QD IgG control was averaged (Figure 10). The Ab–QD probe signal ratios over the IgG control were 0.81 for MMP9, 2.4 for MMP14, and 3.0 for CEA. Only MMP14 and CEA probes successfully identified the tumor. The human tissue results were surprisingly different from those of the AOM/DSS mouse model stained *ex vivo* or *in vivo*. For the mouse model, the MMP9 and MMP14 probes showed a 2-fold signal ratio over the IgG controls, while the CEA probe failed to identify the tumor sites. In human colon cancer studies, the CEA expression level has been reported to be a maximum of 10.8-fold higher for patients with colorectal cancer than the control.[28] MMP9 and MMP14 are known to participate in tumor growth and metastasis at advancing stages in human colon carcinoma,[47] and a patient derived xenograft mouse model showed strongly expressed MMP9 in colon carcinomas. We do not have a convincing explanation on why the MMP14 and CEA probes worked for the human specimen and not for the MMP9 probe. It could be due to the cancer inhomogeneity where the polyps, which were pathologically identified as adenoma, were at the stage of different expression levels of MMP9 and MMP14.

CONCLUSIONS

We report the combination of QD probes with a simultaneous "spray and wash" technique for the diagnosis of colon cancer using endoscopy. After the QD probe treatments, the nonspecific bound QDs can be reduced by the washing step as the antifouling zwitterionic surface coating minimized the interaction with the tissue. Targeted QD probes are likely to be eliminated from the body along with the excised tissues for biopsy and the toxicity issue can be greatly mitigated. Our Ab–QD probes showed the potential for rapid and accurate diagnoses on sectioned mouse tissues, fresh mouse colons stained *ex vivo* and also *in vivo*. Two photon microscopic imaging was used to characterize the probe distribution at different depths. For a one-time 30 min staining, the multi-Ab–QD probes successfully identified tumors with high signal ratios over the IgG control probe. The staining depth could reach over 100 μm. The probe distribution from the surface provided a high enough optical signal to identify the tumors. However, considering our mouse tumor sizes up to 5 mm, ~100 μm probe penetration may seem superficial and our Ab–QD probes can bind biomarkers mostly in the upper mucosa layers. This makes our probes relatively more sensitive to small tumors such as microtumors than larger ones that are readily discernible by bare eyes *via* endoscopy. The MMP9, MMP14, and CEA probes showed different signal levels between the FFPE sectioned tissues and fresh colons. This may have originated from the probe distribution as sprayed probes on colons have to permeate from the surface while it is not the case for the sectioned tissues. All three probes were highly populated for sectioned tumor tissues, whereas only MMP9 and MMP14 probes successfully identified tumors in fresh colons. Multiplexed and simultaneously stained images were further exploited by postprocesses such as sum and cross operations.

The postprocessed images can add new dimensions in diagnoses when they are data-based from many patients, and are expected to aid surgeons for accurate, real-time, and on-spot detection of cancer for biopsy and/or resection with minimized risk of false negative and false positive errors. Multi-Ab–QD probes were further applied to fresh human colon adenoma tissues, where MMP14 and CEA probes showed successful diagnoses of cancer at their early stages. The MMP9 probe did not work as expected for the human specimen, which also stresses the importance of multiplexed diagnosis for cancer. In principle, QDs are well suited for multiplexing and can easily provide over 20 different emission colors spanning the visible and near-infrared. The high degree of multiplexing of QDs is important as cancer cells express many different biomarkers and no single markers can show 100% accuracy for diagnosis due to the heterogeneity of cancer. There are some remaining challenges of the "spray and wash" type staining such as penetration depth, tissue-specificity, and the washing-step dependence. Nonetheless, the topical administration is considered to be advantageous for rapid small tumor detection in field that can easily fail by conventional endoscopic examinations.

EXPERIMENTAL SECTION

Materials and Instruments. *N*-(3-(Dimethylamino)propyl)-*N*′-ethylcarbodiimide hydrochloride (EDC, commercial grade) and *N*-hydroxysulfosuccinimide sodium salt (S-NHS, 98.5%) were purchased from Sigma-Aldrich. Anti-MMP9(sc-6840 from Santa Cruz Biotechnology) and MMP14 (Ab-53712 from Abcam) antibodies were used for mouse and human tissues. In the case of anti-CEA, sc-8225 from Santa Cruz Biotechnology was used for mouse tissues and ab-33562 from Abcam was used for human specimen. Normal rabbit IgG (sc-2027) and normal goat IgG (sc-2028) were purchased from Santa Cruz Biotechnology. Water was triply distilled using Millipore filtration system. Absorption spectra were obtained using an Agilent 8453. Photoluminescence (PL) spectra were obtained using HORIBA FluoroLog. Particle hydrodynamic (HD) sizes were measured by Malvern Zetasizer S.

Synthesis of Quantum Dots, Antibody–Quantum Dots Conjugates, and MMP14 Antibody-Rhodamine B Conjugates. CdSe/CdS/ZnS (Core/Shell/Shell) QDs with the emission peak at 560, 585, and 630 nm were synthesized using the procedures previously published.[25] QD's surface was codecorated by zwitterions and carboxylates by surface ligand exchange procedures previously reported elsewhere.[25] 1-Ethyl-3-(3-(dimethylamino)propyl)carbodiimide (EDC, 100 equiv to QDs) and *N*-hydroxysulfosuccinimide (S-NHS, 200 equiv to QDs) were added to mixed-ligand exchanged QDs with zwitterionic ligand and carboxylate ligand (the ratio of zwitterionic ligand to carboxylate ligand was 1:1) in 50 mM 2-(*N*-morpholino)ethanesulfonic acid (MES) buffer. After 10 min vortexing, the excess EDC and S-NHS were dialyzed using MES buffer and deionized water. Finally, antibodies in 0.1 M pH 7.4 phosphate buffer solution (PBS) were added to the EDC/S-NHS activated QD solution. The final volume of the QD solution was less than 100 μL. The reaction incubated for 2 h at room temperature (RT) on a shaker. After conjugation, Ab–QD conjugates were purified with PBS buffer by 50 kDa centrifugal filter. MMP14–Rhodamine B conjugates were synthesized with NHS-Rhodamine B (46406 from Thermo Scientific) and anti-MMP14(Ab-53712 from Abcam) antibody. NHS–Rhodamine B was dissolved in dimethyl sulfoxide (DMSO) and stirred thoroughly. The NHS–Rhodamine B solution was added to the anti-MMP14 antibody PBS buffer solution, making the solution about 1% DMSO in PBS. The reaction mixture was stirred well at room temperature for 1 h. The reaction ratio of the dye to antibody was 10-fold molar excess. After the reaction, nonreacted NHS–Rhodamine B was removed by gel filtration.

AOM/DSS Model and Histology. Four week male BALB/c (Charles River Laboratories Japan, Inc.,Yokohama, Japan) mice were acclimatized for 7 days to tap water and an *ad libitum* basal diet. The mice were given a single intraperitoneal injection of Azoxymethane (AOM; 10 mg/kg body weight; Sigma–Aldrich). One week later, animals were administered 2% (w/v) dextran sulfate sodium (DSS; molecular weight 36 000–50 000) for 7 days *via* the drinking water, followed by maintenance on a basal diet and tap water for 14 days. This administration of DSS in the drinking water was repeated. Colonoscopy (Karl Storz, Tuttlingen, Germany) was performed in AOM/DSS model to check whether colon tumors were formed adequately. The mice were sacrificed at 4 weeks after the end of DSS administration. All animal experiments were performed with protocols approved by the Institutional Animal Care and Use Committee (IACUC) of the Asan Institute for Life Sciences at the Asan Medical Center, consistent with the Institute of Laboratory Animal Resources (ILAR) guide. The colons of AOM/DSS treated mice were removed, flushed with PBS, and dissected longitudinally. For histological analysis, the tissues were fixed in 10% formalin and embedded in paraffin. Four-micrometer-thick sections were stained with H&E using routine procedure. Histological analysis was performed by one gastrointestinal pathologist.

Ab–QD Probe Staining for Sectioned AOM/DSS Mouse Colon Tissues. Formalin-fixed paraffin-embedded tissue sections were preheated at 60 °C for 30 min and were then deparaffinized by immersion in xylene two times for 30 min, respectively. Tissue hydration was carried out by a series of immersion steps at decreasing ethanol concentrations (99, 95 and 80% ethanol for 5, 10, and 5 min, respectively), followed by rinsing in water for 5 min. Antigen retrieval was performed at 100 °C for 1 h in 10 mM citrate buffer. After the tissues had cooled, the tissue slides were washed by DI water. Four Ab–QDs were prepared using 630 nm emitting QDs conjugating to CEA, MMP9, MMP14, or normal immunoglobulin G (IgG) control. The concentration of probe solution was 1 μM, respectively, and then incubation for 1 h at room temperature. After the tissue slides were wash, they were mounted with 4,6-diamidino-2-phenylindole (DAPI, Vector Laboratories, Burlingame, CA) to stain nuclei. Dehydration and mounting on coverslips were performed for fluorescence imaging. Fluorescence microscope images were recorded using a Zeiss Axioplan. For QD excitation, 455/30 nm band-pass filter was used when the images were recorded with a 515 nm long pass filter and 405/40 nm band-pass filter was used when the images were obtained with a 625/30 nm band-pass filter to visualize the fluorescence signal from the QDs. The integration time was equal in same slide of tumor and normal tissue.

Mouse Colon Tissue Imaging by "Spray and Wash" Ab–QD Probe *ex Vivo* Staining. Fresh intact colon tissues were obtained from AOM/DSS mouse model by surgically excising and longitudinally cutting to expose the mucosa layer of colon immediately after the sacrifice. Five mice were sacrificed for each biomarker experimental set to display two whole colons stained by the control IgG–QD conjugate and three colons stained by the Ab–QD probe, respectively. Three different color emitting QDs were used for the Ab conjugation: MMP9 Ab conjugated to 630QD, MMP14 Ab conjugated to 585QD, and CEA Ab conjugated to 560QD. Normal IgG QD conjugates were also prepared for the control with each three QDs. The fresh colon tissues were sprayed by 500 nM Ab–QD conjugate probe PBS solution.

The PBS probe solution was sprayed using micropipettes by rapidly ejecting small portions of the probe solution to evenly coat the colon mucosa layer surfaces that had been longitudinally cut open. The specimen was incubated for 30 min, and washed with PBS buffer for 15 min. The colon tissues were laid down with the mucosa layer facing up and brought into the IVIS system. The rainbow fluorescence signal, expressed at the colon tissue, was obtained using the Xenogen IVIS spectrum system (Caliper Life Science, Inc., Hopkinton, MA). Images were acquired with excitation at 430 nm and emission at 500−800 nm using auto acquisition, a binning factor of 8 and field of view of 13.4 cm. Fluorescence imaging were processed with spectral unmixing using the Living Image 4.3.1 software (Caliper Life Sciences, Hopkinton, MA) to distinguish the autofluorescence and fluorescence of QD probes. The region of interest (ROI) of each tissues has been selected by manually following the boundary of each tissues. For normalized data, we quantified the fluorescence to the radiant efficiency. For multi-Ab−QD probe staining, the 500 nM MMP9−630QD, MMP14−585QD, and CEA−560QD solutions were mixed in equal volumes. The final concentration of each probe was 167 nM. As a control to the multi-Ab−QD probe mixture, multi-IgG−QD control probe was prepared by the mixture of IgG conjugates to 560QD, 585QD, and 630QD. Using the mixture probe solution, the fresh colon staining experiment was repeated. IVIS spectral imaging was used to measure each probe signal (Supporting Information Figure S18). To unmix each probe signal form multi-QD probes stained tissues, fluorescence spectra for each single QD probe and unstained mouse colon tissues were obtained using IVIS system (Supporting Information Figure S19). Spectral unmixing was performed to eliminate the tissue autofluorescence and cross-talks from different color QD probes. The spectral unmixing was based on multivariate curve resolution (MCR) method,[48] and provided by the Living Image 4.3.1 software for IVIS. Raw fluorescence data was discretized to a matrix form $\mathbf{CS} + \mathbf{R}$, where **C** represents the composition of the mixed fluorophores at the corresponding pixel, **S** represents pure spectrum of each fluorophores, and **R** means error term. Using the spectra of probes and unstained tissues, as the initial value, iteration was performed to solve the least-squares problem and find proper **C** and **S** matrices. In addition, several constrains were applied to generate meaningful solution, such as non-negativity of the matrices since the contribution or concentration of fluorophores cannot be negative.

Two-Photon Microscopic Imaging of the *ex Vivo* Stained Colon Tissues. Multi-Ab−QD probes stained tissue was spread on glass slide and covered with cover glass. Two-photon microscope (TCS SP5 II, Leica) with a Ti-Sapphire laser (Chameleon Vision II, Coherent) at 140 fs pulse width and 80 MHz pulse repetition rate was used. 3D imaging was performed by using a 20× objective lenses (HCX IRAPO L20x, NA 1.0 W, Leica) with the stepwise increment of 2 μm in the depth direction. The excitation laser was tuned to 780 and 980 nm for tissue autofluorescence and QDs fluorescence signals, respectively. The emission light of each Ab−QD probe was spectrally resolved into 4 channels by using a set of dichroic mirrors at 495 nm, 560 and 620 nm and band-pass filter 562/40 for 560QDs, 586/20 for 585QDs, 624/40 for 630QDs. QD signals were obtained through the band passes of 544−560 nm for 560QD, 576−596 nm for 585QD and 620−644 nm for 630QD. 3D images were acquired by taking multiple $x-y$ plane images with stepwise increment of 2 μm in the z-direction from the colonic tissue surface to a depth of 200 μm. Power of the excitation laser was approximately 10 mW on the tissue surface, and increased with depth in order to maintain the signal-to-noise ratio. The imaging field-of-view was 250 μm × 250 μm consisting of 512 × 512 pixels, and the imaging speed was 0.78 frames/s. Acquired images were processed by using LAS AF Lite (Leica).

Postimage Processes Using Sum Operation and Cross Operation. Image data process was conducted using the MATLAB (The MatWorks, Inc.) program. The raw radiant efficiency image of multi-Ab−QD probes stained tissues were imported to MATLAB as matrix. The each element of matrix was composed of image pixels. Each probe has different QD absorbance, quantum efficiency and detector sensitivity, so these differences were normalized to compare the number of stained probe. Each single probe (100 nM) was placed on 96-well plate and radiant efficiency was measured by IVIS spectrum, and the raw radiant efficiency data of tissues on each probe channel were divided by the radiant efficiency of each probe. For the sum operation, normalized radiant intensities for different images were added for the same position pixel by pixel. For the cross operation, the elements at the same position were multiplied. The calculated elements were converted to pixels of image which was expressed by rainbow color map. The threshold was obtained by the global thresholding algorithm using a MATLAB program that we had previously reported.[49]

Mouse Colon Tissue Imaging by "Spray and Wash" Ab−QD Probe *in Vivo* Staining and Two-Photon Microscopic Imaging. To incubate multi-Ab−QD probes *in vivo*, the mouse was anesthetized by inhaling isoflurane during the experiment. Multi-Ab−QD probes (100 nM) were filled in a syringe with a pliable plastic gavage needle. Then, the needle was pulled out slowly during spraying the multi-Ab−QD probes. The isoflurane insufflation was removed right after the spraying. After 30 min, the mouse was sacrificed and the colon was excised and washed with PBS buffer for 15 min.

Human Colon Tissue Imaging by "Spray and Wash" Ab−QD Probes. A colon adenoma excised from transverse colon of a patient was cut in half to compare the multi-Ab−QD probe staining with the case of multi-IgG−QD control probe. A 330 nM multi-Ab−QD mixture probe solution was sprayed onto the tissues, and the sample was incubated for 60 min, followed by washing for 3 min. Fluorescence image obtained using the Xenogen IVIS spectrum system (Caliper Life Science, Inc., Hopkinton, MA). Images were acquired with excitation at 430 nm and emission at 500−800 nm using auto acquisition, a binning factor of 8 and field of view of 6.6 cm. Fluorescence imaging were processed spectral unmixing using the Living Image 4.3.1 software (Caliper Life Sciences, Hopkinton, MA) and quantifying the image as the radiant efficiency. We repeated the experiments three times and all colon tissues were confirmed to have tubular adenomas which were from sigmoid and ascending colon.

Conflict of Interest: The authors declare no competing financial interest.

Supporting Information Available: Additional experimental data and movies (.avi). This material is available free of charge *via* the Internet at http://pubs.acs.org.

Acknowledgment. This research was supported by the Bio & Medical Technology Development Program of the National Research Foundation (NRF) funded by the Korean government (MOST) (2011-0019632, 2011-0019633, 2011-0019635). We appreciate the technical assistance of Hoe-Yune, Jung with the use of the IVIS spectrum facility supported by the Pohang Center for Evaluation of Biomaterials (Pohang Technopark).

REFERENCES AND NOTES

1. Siegel, R.; Naishadham, D.; Jemal, A. Cancer Statistics, 2013. *Ca−Cancer J. Clin.* **2013**, *63*, 11–30.
2. Lieberman, D. A. Screening for Colorectal Cancer. *N. Engl. J. Med.* **2009**, *361*, 1179–1187.
3. Nishihara, R.; Wu, K.; Lochhead, P.; Morikawa, T.; Liao, X.; Qian, Z. R.; Inamura, K.; Kim, S. A.; Kuchiba, A.; Yamauchi, M.; *et al.* Long-Term Colorectal-Cancer Incidence and Mortality after Lower Endoscopy. *N. Engl. J. Med.* **2013**, *369*, 1095–1105.
4. Heresbach, D.; Barrioz, T.; Lapalus, M. G.; Coumaros, D.; Bauret, P.; Potier, P.; Sautereau, D.; Boustière, C.; Grimaud, J. C.; Barthélémy, C.; *et al.* Miss Rate for Colorectal Neoplastic Polyps: a Prospective Multicenter Study of Back-to-back Video Colonoscopies. *Endoscopy* **2008**, *40*, 284–290.
5. Konishi, K.; Kaneko, K.; Kurahashi, T.; Yamamoto, T.; Kushima, M.; Kanda, A.; Tajiri, H.; Mitamura, K. A Comparison of Magnifying and Nonmagnifying Colonoscopy for Diagnosis of Colorectal Polyps: A Prospective Study. *Gastrointest. Endosc.* **2003**, *57*, 48–53.

6. Hurlstone, D. P.; Fujii, T. Practical Uses of Chromoendoscopy and Magnification at Colonoscopy. *Gastrointest. Endosc. Clin. N. Am.* **2005**, *15*, 687–702.
7. Chiu, H.-M.; Chang, C.-Y.; Chen, C.-C.; Lee, Y.-C.; Wu, M.-S.; Lin, J.-T.; Shun, C.-T.; Wang, H.-P. A Prospective Comparative Study of Narrow-Band Imaging, Chromoendoscopy, and Conventional Colonoscopy in the Diagnosis of Colorectal Neoplasia. *Gut* **2007**, *56*, 373–379.
8. Pasha, S. F.; Leighton, J. A.; Das, A.; Harrison, M. E.; Gurudu, S. R.; Ramirez, F. C.; Fleischer, D. E.; Sharma, V. K. Comparison of the Yield and Miss Rate of Narrow Band Imaging and White Light Endoscopy in Patients Undergoing Screening or Surveillance Colonoscopy: A Meta-Analysis. *Am. J. Gastroenterol.* **2012**, *107*, 363–370.
9. Garai, E.; Sensarn, S.; Zavaleta, C. L.; Van de Sompel, D.; Loewke, N. O.; Mandella, M. J.; Gambhir, S. S.; Contag, C. H. High-sensitivity, Real-time, Ratiometric imaging of Surface-enhanced Raman Scattering Nanoparticles with a Clinically Translatable Raman Endoscope Device. *J. Biomed. Opt.* **2013**, *18*, 096008.
10. Zavaleta, C. L.; Hartman, K. B.; Miao, Z.; James, M. L.; Kempen, P.; Thakor, A. S.; Nielsen, C. H.; Sinclair, R.; Cheng, Z.; Gambhir, S. S. Preclinical Evaluation of Raman Nanoparticle Biodistribution for Their Potential Use in Clinical Endoscopy Imaging. *Small* **2011**, *7*, 2232–2240.
11. Miller, S. J.; Joshi, B. P.; Feng, Y.; Gaustad, A.; Fearon, E. R.; Wang, T. D. *In Vivo* Fluorescence-Based Endoscopic Detection of Colon Dysplasia in the Mouse Using a Novel Peptide Probe. *PLoS One* **2011**, *6*, e17384.
12. Bruchez, M.; Moronne, M.; Gin, P.; Weiss, S.; Alivisatos, A. P. Semiconductor Nanocrystals as Fluorescent Biological Labels. *Science* **1998**, *281*, 2013–2016.
13. Chan, W. C. W.; Nie, S. Quantum Dot Bioconjugates for Ultrasensitive Nonisotopic Detection. *Science* **1998**, *281*, 2016–2018.
14. Medintz, I. L.; Uyeda, H. T.; Goldman, E. R.; Mattoussi, H. Quantum Dot Bioconjugates for Imaging, Labelling and Sensing. *Nat. Mater.* **2005**, *4*, 435–446.
15. Deka, S.; Quarta, A.; Lupo, M. G.; Falqui, A.; Boninelli, S.; Giannini, C.; Morello, G.; De Giorgi, M.; Lanzani, G.; Spinella, C.; *et al.* CdSe/CdS/ZnS Double Shell Nanorods with High Photoluminescence Efficiency and Their Exploitation as Biolabeling Probes. *J. Am. Chem. Soc.* **2009**, *131*, 2948–2958.
16. Wegner, K. D.; Jin, Z.; Lindén, S.; Jennings, T. L.; Hildebrandt, N. Quantum-Dot-Based Förster Resonance Energy Transfer Immunoassay for Sensitive Clinical Diagnostics of Low-Volume Serum Samples. *ACS Nano* **2013**, *7*, 7411–7419.
17. Farlow, J.; Seo, D.; Broaders, K. E.; Taylor, M. J.; Gartner, Z. J.; Jun, Y.-w. Formation of Targeted Monovalent Quantum Dots by Steric Exclusion. *Nat. Methods* **2013**, *10*, 1203–1205.
18. Chen, C.; Peng, J.; Xia, H.-S.; Yang, G.-F.; Wu, Q.-S.; Chen, L.-D.; Zeng, L.-B.; Zhang, Z.-L.; Pang, D.-W.; Li, Y. Quantum Dots-Based Immunofluorescence Technology for the Quantitative Determination of HER2 Expression in Breast Cancer. *Biomaterials* **2009**, *30*, 2912–2918.
19. Liu, X.-L.; Peng, C.-W.; Chen, C.; Yang, X.-Q.; Hu, M.-B.; Xia, H.-S.; Liu, S.-P.; Pang, D.-W.; Li, Y. Quantum Dots-Based Double-Color Imaging of HER2 Positive Breast Cancer Invasion. *Biochem. Biophys. Res. Commun.* **2011**, *409*, 577–582.
20. Sweeney, E.; Ward, T. H.; Gray, N.; Womack, C.; Jayson, G.; Hughes, A.; Dive, C.; Byers, R. Quantitative Multiplexed Quantum Dot Immunohistochemistry. *Biochem. Biophys. Res. Commun.* **2008**, *374*, 181–186.
21. Huang, D.-h.; Su, L.; Peng, X.-h.; Zhang, H.; Khuri, F. R.; Shin, D. M.; Chen, Z. Quantum Dot-Based Quantification Revealed Differences in Subcellular Localization of EGFR and E-Cadherin Between EGFR-TKI Sensitive and Insensitive Cancer Cells. *Nanotechnology* **2009**, *20*, 225102.
22. Yezhelyev, M. V.; Al-Hajj, A.; Morris, C.; Marcus, A. I.; Liu, T.; Lewis, M.; Cohen, C.; Zrazhevskiy, P.; Simons, J. W.; Rogatko, A.; *et al. In Situ* Molecular Profiling of Breast Cancer Biomarkers with Multicolor Quantum Dots. *Adv. Mater.* **2007**, *19*, 3146–3151.
23. Liu, J.; Lau, S. K.; Varma, V. A.; Moffitt, R. A.; Caldwell, M.; Liu, T.; Young, A. N.; Petros, J. A.; Osunkoya, A. O.; Krogstad, T.; *et al.* Molecular Mapping of Tumor Heterogeneity on Clinical Tissue Specimens with Multiplexed Quantum Dots. *ACS Nano* **2010**, *4*, 2755–2765.
24. Xu, H.; Xu, J.; Wang, X.; Wu, D.; Chen, Z. G.; Wang, A. Y. Quantum Dot-Based, Quantitative, and Multiplexed Assay for Tissue Staining. *ACS Appl. Mater. Interfaces* **2013**, *5*, 2901–2907.
25. Park, J.; Nam, J.; Won, N.; Jin, H.; Jung, S.; Jung, S.; Cho, S.-H.; Kim, S. Compact and Stable Quantum Dots with Positive, Negative, or Zwitterionic Surface: Specific Cell Interactions and Non-Specific Adsorptions by the Surface Charges. *Adv. Funct. Mater.* **2011**, *21*, 1558–1566.
26. Park, J.; Park, Y.; Kim, S. Signal Amplification *via* Biological Self-Assembly of Surface-Engineered Quantum Dots for Multiplexed Subattomolar Immunoassays and Apoptosis Imaging. *ACS Nano* **2013**, *7*, 9416–9427.
27. Hussain, S.; Won, N.; Nam, J.; Bang, J.; Chung, H.; Kim, S. One-Pot Fabrication of High-Quality InP/ZnS (Core/Shell) Quantum Dots and Their Application to Cellular Imaging. *ChemPhysChem* **2009**, *10*, 1466–1470.
28. Bang, J.; Park, J.; Lee, J. H.; Won, N.; Nam, J.; Lim, J.; Chang, B. Y.; Lee, H. J.; Chon, B.; Shin, J.; *et al.* ZnTe/ZnSe (Core/Shell) Type-II Quantum Dots: Their Optical and Photovoltaic Properties. *Chem. Mater.* **2010**, *22*, 233–240.
29. Zhang, Y.; Hong, G.; Zhang, Y.; Chen, G.; Li, F.; Dai, H.; Wang, Q. Ag_2S Quantum Dot: A Bright and Biocompatible Fluorescent Nanoprobe in the Second Near-Infrared Window. *ACS Nano* **2012**, *6*, 3695–3702.
30. Mook, O. R. F.; Frederiks, W. M.; Van Noorden, C. J. F. The Role of Gelatinases in Colorectal Cancer Progression and Metastasis. *Biochim. Biophys. Acta, Rev. Cancer* **2004**, *1705*, 69–89.
31. Lubbe, W. J.; Zhou, Z. Y.; Fu, W.; Zuzga, D.; Schulz, S.; Fridman, R.; Muschel, R. J.; Waldman, S. A.; Pitari, G. M. Tumor Epithelial Cell Matrix Metalloproteinase 9 Is a Target for Antimetastatic Therapy in Colorectal Cancer. *Clin. Cancer Res.* **2006**, *12*, 1876–1882.
32. Yoon, S. M.; Myung, S. J.; Ye, B. D.; Kim, I. W.; Lee, N. G.; Ryu, Y. M.; Park, K.; Kim, K.; Kwon, I. C.; Park, Y. S.; *et al.* Near-Infrared Fluorescence Imaging Using a Protease-Specific Probe for the Detection of Colon Tumors. *Gut Liver* **2010**, *4*, 488–497.
33. Tiernan, J. P.; Perry, S. L.; Verghese, E. T.; West, N. P.; Yeluri, S.; Jayne, D. G.; Hughes, T. A. Carcinoembryonic Antigen is the Preferred Biomarker for *in Vivo* Colorectal Cancer Targeting. *Br. J. Cancer* **2013**, *108*, 662–667.
34. Zucker, S.; Vacirca, J. Role of Matrix Metalloproteinases (MMPs) in Colorectal Cancer. *Cancer. Metast. Rev.* **2004**, *23*, 101–117.
35. Egeblad, M.; Werb, Z. New Functions for the Matrix Metalloproteinases in Cancer Progression. *Nat. Rev.Cancer.* **2002**, *2*, 161–174.
36. Nakamura, T.; Tabuchi, Y.; Nakae, S.; Ohno, M.; Saitoh, Y. Serum Carcinoembryonic Antigen Levels and Proliferating Cell Nuclear Antigen Labeling Index for Patients with Colorectal Carcinoma. Correlation with Tumor Progression and Survival. *Cancer* **1996**, *77*, 1741–1746.
37. Lynch, C. C.; Matrisian, L. M. Matrix Metalloproteinases in Tumor−Host Cell Communication. *Di□erentiation* **2002**, *70*, 561–573.
38. Liabakk, N.-B.; Talbot, I.; Smith, R. A.; Wilkinson, K.; Balkwill, F. Matrix Metalloprotease 2 (MMP-2) and Matrix Metalloprotease 9 (MMP-9) Type IV Collagenases in Colorectal Cancer. *Cancer Res.* **1996**, *56*, 190–196.
39. Malhotra, S.; Newman, E.; Eisenberg, D.; Scholes, J.; Wieczorek, R.; Mignatti, P.; Shamamian, P. Increased Membrane Type 1 Matrix Metalloproteinase Expression from Adenoma to Colon Cancer—A Possible Mechanism of Neoplastic Progression. *Dis. Colon Rectum* **2002**, *45*, 537–543.

40. Ahnen, D. J.; Nakane, P. K.; Brown, W. R. Ultrastructural Localization of Carcinoembryonic Antigen in Normal Intestine and Colon Cancer. Abnormal Distribution of CEA on the Surfaces of Colon Cancer Cells. *Cancer* **1982**, *49*, 2077–2090.
41. Huitric, E.; Laumonier, R.; Burtin, P.; Von Kleist, S.; Chavanel, G. An Optical and Ultrastructural Study of the Localization of Carcinoembryonic Antigen (CEA) in Normal and Cancerous Human Rectocolonic Mucosa. *Lab. Invest.* **1976**, *34*, 97–107.
42. Shang, K.; Bai, Y.-P.; Wang, C.; Wang, Z.; Gu, H.-Y.; Du, X.; Zhou, X.-Y.; Zheng, C.-L.; Chi, Y.-Y.; Mukaida, N.; *et al.* Crucial Involvement of Tumor-Associated Neutrophils in the Regulation of Chronic Colitis-Associated Carcinogenesis in Mice. *PLoS One* **2012**, *7*, e51848.
43. Suzuki, R.; Miyamoto, S.; Yasui, Y.; Sugie, S.; Tanaka, T. Global Gene Expression Analysis of the Mouse Colonic Mucosa Treated with Azoxymethane and Dextran Sodium Sulfate. *BMC Cancer* **2007**, *7*, 84.
44. Tobioka, H.; Isomura, H.; Kokai, Y.; Sawada, N. Polarized Distribution of Carcinoembryonic Antigen Is Associated with a Tight Junction Molecule in Human Colorectal Adenocarcinoma. *J. Pathol.* **2002**, *198*, 207–212.
45. Kaihara, T.; Kawamata, H.; Imura, J.; Fujii, S.; Kitajima, K.; Omotehara, F.; Maeda, N.; Nakamura, T.; Fujimori, T. Redifferentiation and ZO-1 Reexpression in Liver-metastasized Colorectal Cancer: Possible Association with Epidermal Growth Factor Receptor-induced Tyrosine Phosphorylation of ZO-1. *Cancer Sci.* **2003**, *94*, 166–172.
46. Soler, A. P.; Miller, R. D.; Laughlin, K. V.; Carp, N. Z.; Klurfeld, D. M.; Mullin, J. M. Increased Tight Junctional Permeability is Associated with the Development of colon cancer. *Carcinogenesis* **1999**, *20*, 1425–1431.
47. Matsuyama, Y.; Takao, S.; Aikou, T. Comparison of Matrix Metalloproteinase Expression between Primary Tumors with or without Liver Metastasis in Pancreatic and Colorectal Carcinomas. *J. Surg. Oncology.* **2002**, *80*, 105–110.
48. Xu, H.; Rice, B. W. *In Vivo* Fluorescence Imaging with a Multivariate Curve Resolution Spectral Unmixing Technique. *J. Biomed. Opt.* **2009**, *14*, 064011.
49. Won, N.; Jeong, S.; Kim, K.; Kwag, J.; Park, J.; Kim, S. G.; Kim, S. Imaging Depths of Near-Infrared Quantum Dots in First and Second Optical Windows. *Mol. Imaging* **2012**, *11*, 338–352.